




# Photoelectrochemical response of non-enzymatic glucose biosensing for graphene, carbon nanotubes and BiVO<sub>4</sub> nanocomposites

Syeda Ammara Shabbir<sup>1,\*</sup> , Ambreen Imran<sup>1</sup>, Muhammad Gul Bahar Ashiq<sup>2</sup>, Hamid Latif<sup>1</sup>, Khalid Javed<sup>1</sup>, and Mahroze Munam<sup>1</sup>

<sup>1</sup>Department of Physics, Forman Christian College (A Chartered University), Lahore 54600, Pakistan

<sup>2</sup>Department of Physics, College of Science, Imam Abdulrahman Bin Faisal University, P.O. Box 1982, Dammam 31441, Saudi Arabia

Received: 24 March 2021

Accepted: 30 May 2021

Published online:  
17 June 2021

© The Author(s), under exclusive licence to Springer Science+Business Media, LLC, part of Springer Nature 2021

## ABSTRACT

Diabetes mellitus is a worldwide disease which affects the vital organs of human body. The approach executed in this project is to fabricate the nanocomposites of BiVO<sub>4</sub> by incorporating reduced graphene oxide (RGO) and carbon nanotubes (CNT) for photoelectrochemical non-enzymatic glucose detection. These different composites were prepared using electrochemical deposition method. X-ray Diffraction (XRD) and scanning electron microscope (SEM) analysis confirmed the structural details and surface morphology of these nanostructures, graphene sheet, BiVO<sub>4</sub> nanoparticles and of carbon nanotubes. UV–Vis analysis revealed the increasing trend in absorption of light and absorption edge, for BiVO<sub>4</sub>, CNT/BiVO<sub>4</sub>, RGO/BiVO<sub>4</sub> and CNT/RGO/BiVO<sub>4</sub> electrodes, respectively. The photoelectrochemical response was measured through Linear Sweep voltammetry and increase in current density was observed from pure BiVO<sub>4</sub> nanoparticles to CNT/BiVO<sub>4</sub> to RGO/BiVO<sub>4</sub> and to CNT/RGO/BiVO<sub>4</sub>, due to incorporation of graphene and carbon nanotubes. The increasing glucose oxidation current was measured through cyclic voltammetry. It was observed that glucose oxidation peak was maximum for CNT/RGO/BiVO<sub>4</sub> electrode, as the incorporation of extremely conductive CNTs specifies several routes for the transportation of electrons and act as an impressive conductive binders to restrict the agglomeration of graphene nanosheets, thus enhancing the rate of electrons exchange. This study shows that CNT/RGO/BiVO<sub>4</sub> electrode is the best photoelectrochemical electrode for non-enzymatic glucose detection for providing maximum sensitivity of 501.5 mA cm<sup>-2</sup> mM<sup>-1</sup> and good stability with negligible current response from interference species.

Address correspondence to E-mail: ammaraanwar@fccollege.edu.pk

## 1 Introduction

Diabetes mellitus is an international public health issue, which is caused by the shortage of insulin and excess of glucose in the blood [1]. This disease is the major cause of vital body organs failure. Therefore, regular glucose monitoring is integral to know whether medicines are working successfully [2]. Blood glucose meters are usually based on enzymatic biosensors in which minor pin pricks are used to obtain blood for glucose detection. Enzymes are unstable as they lose their activity after a short period of time or they become denature with the variation in temperature. Enzymes are costly and depend upon ambient humidity levels. However, non-enzymatic biosensors are more stable and detects glucose through direct oxidation in the specimen. For regular glucose monitoring, non-enzymatic biosensors [3, 4] are preferred. In order to make sure that sufficient insulin is given off at proper time, a regular monitoring system traces out correct quantity of glucose round the clock. Non-enzymatic biosensors also have some drawbacks. They are highly sensitive towards electroactive interfering species present in the blood. Metal electrodes can easily be poisoned by adsorbed intermediates present in the blood.

Due to these disadvantages, research trend is leading towards photoelectrochemical (PEC) biosensing for the detection of biomolecules [5–8]. Photoelectrochemical sensing is a low cost detection method and provides higher sensitivity. Efficiency of PEC sensor depends upon the photo catalytic ability of active material. It involves electron transfer reaction amongst photo active material, the electrode and the anode, when light falls on it [1, 9, 10]. PEC Sensors has the ability to combine the process of photo excitation and electrochemical detection, and this feature makes it more useful as electrochemical and optical sensors. Photoelectrochemical non-enzymatic biosensors comprising composites of GR-CdS quantum dots were successfully fabricated [11, 12]. Some other nanomaterials such as TiO<sub>2</sub>-B nanorods graphene decorated with CdS, TiC-C nanoflower, Cu<sub>2</sub>O<sub>2</sub>-TiO<sub>2</sub>, nanohybrid sheets of Bismuth oxychloride BiOCl-graphene have been utilized for non-enzymatic photoelectrochemical glucose biosensing [13–15].

Bismuth Vanadate has been given an extreme importance by the researchers, due to its less toxicity, high chemical stability, and small bandgap of about

2.4 eV. Researchers have also found that BiVO<sub>4</sub> shows excellent photocatalytic properties [16–19]. Properties of narrow bandgap facilitate the formation of photo induced charge carrier. The photogenerated holes of BiVO<sub>4</sub> have a strong capability to oxidize organic matter that is attached to the surface, however, further research needs to explore in the area of application in non-enzymatic glucose sensors. Gopalan et al. [13, 20], successfully developed non-enzymatic photoelectrochemical glucose biosensor produced with the help of BiVO<sub>4</sub> electrode under visible light. However, due to insufficient transfer of charged particles and poorly adsorbed surface, the rate of recombination of electron-hole pair was high and thus it limited the photocatalytic properties of pure BiVO<sub>4</sub> [21]. Therefore to enhance the photocatalytic properties of BiVO<sub>4</sub>, researchers explored different approaches like control of crystal Structure, combining with metal-oxides [22], non-metal doping [23] and noble metal deposition [24]. Carbon nanotubes being one dimensional material provide high conductivity with faster electron transfer rate. As graphene possesses distinctive nanostructure and exceptional properties, therefore graphene-based compounds have been the centre of attraction. Graphene-based compounds have been developed for different approaches like optical devices, sensors, catalysts. Graphene/TiO<sub>2</sub> nanocomposite was developed by Dai and his Co-workers, to show exceptional photocatalytic action in the degradation of Rhodamine B. Composite of Graphene/PtRu have been synthesized showing excellent electrocatalytic performance for methanol oxidation. The composite of BiVO<sub>4</sub>/rGO was developed to show the improved photocatalytic action in the degradation of RhB, by Xiong [25]. BiVO<sub>4</sub>/rGO composite synthesized, by Yun Hau Na et al. as photocatalyst to exhibit improved photoelectrochemical effect in water splitting [26–28]. Therefore in this research project, the non-enzymatic photoelectrochemical glucose biosensing response of the electrodes based on composites of RGO, CNT and BiVO<sub>4</sub> nanoparticles, under visible light has been analyzed for the first time.

## 2 Experimentation

### 2.1 Materials

Bismuth Nitrate Pentahydrate ( $\text{Bi}(\text{NO}_3)_3$ ), Potassium Iodide (KI), Nitric Acid ( $\text{HNO}_3$ ), Vanadyl Acetylacetonate ( $\text{VO}(\text{acac})_2$ ), Dimethyl sulfoxide, Sodium Hydroxide (NaOH), COOH functionalized CNTs, sodium dodecyl sulphate (SDS), Hydrazine monohydrate, 1, 4-benzoquinone, Sulphuric acid ( $\text{H}_2\text{SO}_4$ ), Hydrochloric acid (HCl), Sodium Nitrate ( $\text{NaNO}_3$ ), Potassium Permanganate ( $\text{KMnO}_4$ ), Hydrogen peroxide ( $\text{H}_2\text{O}_2$ ) were all purchased from Sigma Aldrich.

### 2.2 Fabrication of $\text{BiVO}_4$ electrode

For the fabrication of nanoporous electrode of  $\text{BiVO}_4$  on the flourine doped tin oxide glass, electrochemical deposition was used. In order to prepare the solution for plating, 40 mM  $\text{Bi}(\text{NO}_3)_3 \cdot 5\text{H}_2\text{O}$  was dissolved in 50 mL aqueous solution of 400 mM KI. Solution of opaque orange color was obtained. In order to calibrate its pH value to 1.75, few drops of dil.  $\text{HNO}_3$  was added. The color of solution changed to transparent red–orange color. This solution was then dissolved with 0.23 M 1,4-benzoquinone in 20 mL of ethanol along with stirring for 10 min. Blackish solution of BiOI was obtained. The sample was prepared at electrodeposition time of 450 s and potential of + 0.13 V. The BiOI electrode was thoroughly washed with DI water and then it was dried in oven for 15 min at 110 °C. Then 0.20 M of Vanadyl acetylacetonate was mixed in 5 mL dimethyl sulfoxide. Solution became emerald green in color. This mixture was drizzled uniformly on BiOI film. Then electrode was washed in DI water and ethanol and dried at room temperature.

### 2.3 Fabrication of CNT/ $\text{BiVO}_4$ nanocomposite electrode

COOH (50 mg) functionalized CNTs were dissolved in Sodium Dodecyl Sulphate (0.075 g) and deionized water (50 mL). The solution was sonicated for 60 min and then centrifuged for 30 min at the rate of 8000 rpm. The resultant product was stable and homogeneous dispersal. This stable solution was then used for carbon nanotubes-based electrodes fabrication using spin coating. The solution was spin coated on FTO substrate at 3000 rpm for 80 s to

fabricate CNT-based electrodes. The CNT film was coated with thickness approximately 1  $\mu\text{m}$ . Afterwards, fabricated CNT electrode was utilized for  $\text{BiVO}_4$  electrodeposition with the same procedure as mentioned above.

### 2.4 Fabrication of RGO/ $\text{BiVO}_4$ nanocomposite electrode

Reduced Graphene oxide (RGO) was obtained by the modified Hummor's method. The reduced graphene oxide solution was spin coated on FTO substrate at 3000 rpm for 80 s with subsequent electrodeposition of  $\text{BiVO}_4$  to fabricated RGO/ $\text{BiVO}_4$  nanocomposite electrode.

### 2.5 Fabrication of CNT/RGO/ $\text{BiVO}_4$ nanocomposite electrode

CNT is coated on FTO with sequential deposition of RGO and  $\text{BiVO}_4$  to get CNT/RGO/ $\text{BiVO}_4$  electrode.

### 2.6 Characterization of nanocomposite electrodes

Scanning electron microscope (SEM) was used to study the morphology of the  $\text{BiVO}_4$ , CNT/ $\text{BiVO}_4$ , RGO/ $\text{BiVO}_4$  and CNT/RGO/ $\text{BiVO}_4$  electrodes. The XRD spectrum was obtained from X-Ray diffractometer using  $\text{CuK}\alpha$  radiation at 40 kV for identification of the required composite materials. The UV–Vis absorption spectra was obtained using the spectrophotometer.

### 2.7 Photoelectrochemical measurements

A 3-electrode system, with Pt as a counter electrode, saturated calomel electrode as reference electrode and the prepared  $\text{BiVO}_4$  nanocomposites-based electrode as working electrodes, was setup for electrochemical measurements. For the Photoelectrochemical measurements 450 W Xe lamp with Am 1.5G filter and intensity of 100  $\text{mW cm}^{-2}$  was used. The working electrodes geometric area of 2  $\text{cm}^2$  was kept constant. The photocatalytic activity of electrodes for glucose oxidation was examined using linear sweep voltammetry (LSV) and cyclic voltammetry (CV). Amperometric measurements were employed to measure the sensitivity, stability,

reproducibility and interference of electrodes for glucose detection.

### 3 Results and discussion

The UV–Vis spectroscopy was conducted to observe the optical properties of the prepared samples of the Bismuth Vanadate composites. The Graphical analysis of UV–vis Spectroscopy of the four samples,  $\text{BiVO}_4$ ,  $\text{CNT}/\text{BiVO}_4$ ,  $\text{RGO}/\text{BiVO}_4$ , and  $\text{CNT}/\text{RGO}/\text{BiVO}_4$  is given in Fig. 1. The UV analysis shows increasing trend in the light absorption, respectively.

The absorption edge has also been calculated from Fig. 1. The  $\text{BiVO}_4$  electrode shows absorption edge at 520 nm,  $\text{CNT}/\text{BiVO}_4$  at 530 nm,  $\text{RGO}/\text{BiVO}_4$  at 560 nm, and  $\text{CNT}/\text{RGO}/\text{BiVO}_4$  at 600 nm. The introduction of CNTs and graphene in pure  $\text{BiVO}_4$  nanoparticles has decreased the bandgap as a result of bond formation between them and thereby creating new energy states in the bandgap of  $\text{BiVO}_4$ . This decrease in bandgap energy is responsible for increase in the absorption of light and absorption edge, respectively.

Bandgap energy is helpful in evaluating the photocatalytic properties. The relation of incident photon energy and absorbance is given by

$$Ah\nu = C(h\nu - E_g)^n$$

whereas absorption coefficient is represented by  $A$ , bandgap energy is represented by  $E_g$ ,  $h$  is the Planck's Constant,  $\nu$  shows the frequency of the incident light,  $C$  is the constant that is related to the mass of

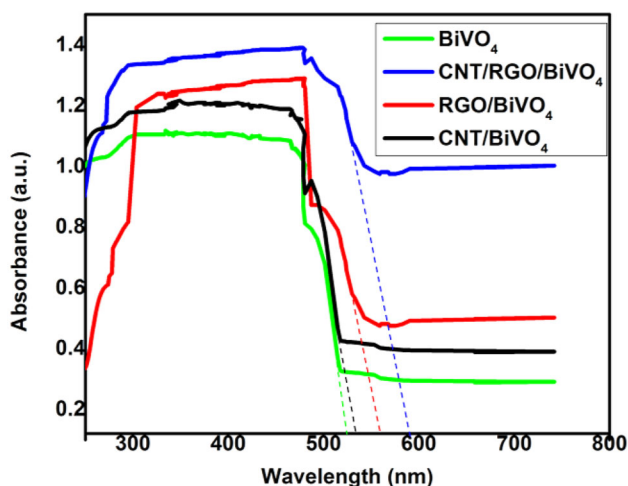


**Fig. 1** UV–vis spectroscopic analysis of  $\text{BiVO}_4$ ,  $\text{CNT}/\text{BiVO}_4$ ,  $\text{RGO}/\text{BiVO}_4$  and  $\text{CNT}/\text{RGO}/\text{BiVO}_4$ , respectively

electrons and holes and the value of  $n$  depends on the type of transition ( $n = 1/2$  for direct transition and  $n = 2$  for indirect transition). The majority of the literature survey suggests that  $\text{BiVO}_4$  follows direct transition. The optical bandgap energies were calculated using the Tauc relation,  $(Ah\nu)^2$  versus  $h\nu$ .

The calculated bandgap energies of pure  $\text{BiVO}_4$  is 2.46 eV, of  $\text{CNT}/\text{BiVO}_4$  is 2.3 eV, of  $\text{RGO}/\text{BiVO}_4$  is 2.16 eV and of  $\text{CNT}/\text{RGO}/\text{BiVO}_4$  is 1.6 eV as shown in Fig. 2. It is observed that incorporation of CNTs, RGO and  $\text{CNT}/\text{RGO}$  with  $\text{BiVO}_4$  has decreased the bandgap energy value from 2.4 to 1.6 eV. Bandgap analysis is correlated with UV analysis. The lowest bandgap energy value of the composite  $\text{CNT}/\text{RGO}/\text{BiVO}_4$  reveals increased absorption of light and increased absorption edge and thus creating more electron–hole pairs for photocatalysis in biosensing (Table 1).

Scanning electron microscope (SEM) was used to determine the surface morphology of the prepared samples of  $\text{BiVO}_4$ ,  $\text{RGO}/\text{BiVO}_4$ ,  $\text{CNT}/\text{BiVO}_4$ , and  $\text{CNT}/\text{RGO}/\text{BiVO}_4$  as shown in Figs. 3, 4, 5 and 6.

The SEM image of  $\text{BiVO}_4$  in Fig. 3a confirms the spherical shape of  $\text{BiVO}_4$  nanoparticles. This image reveals that the particle size ranges from 60 to 70 nm. The SEM image of  $\text{CNT}/\text{BiVO}_4$  composite in Fig. 3b shows tubular structure of carbon nanotubes with attached  $\text{BiVO}_4$  nanoparticles. The SEM image of  $\text{RGO}/\text{BiVO}_4$  composite in Fig. 3c clearly shows that  $\text{BiVO}_4$  nanoparticles are uniformly embedded and well dispersed on the RGO sheets. This embedding of nanoparticles on RGO sheet plays important role in the increased transfer of electrons from  $\text{BiVO}_4$  to RGO after the generation of photogenerated electrons exhibiting improved photocatalytic activity. The SEM image of the  $\text{RGO}/\text{CNT}/\text{BiVO}_4$  composite in Fig. 3d shows graphene sheets wrapping the  $\text{BiVO}_4$  nanoparticles and the entangled CNTs on the surface of graphene sheets prohibits the agglomeration of graphene nano sheets thus enhancing the charge exchange effectively.

The crystal structure analysis of  $\text{BiVO}_4$ ,  $\text{CNT}/\text{BiVO}_4$ ,  $\text{RGO}/\text{BiVO}_4$ , and  $\text{CNT}/\text{RGO}/\text{BiVO}_4$  composites are investigated through XRD analysis. The XRD patterns for all the samples are exhibited in Fig. 4. The sharp diffraction peaks of  $\text{BiVO}_4$  are observed at  $18^\circ$ ,  $28^\circ$ ,  $34^\circ$ ,  $38^\circ$ ,  $52^\circ$ ,  $57^\circ$ ,  $62^\circ$  corresponding to (110), (121), (200), (002), (161), (251), and (132) diffraction planes respectively showing large crystallinity [29].

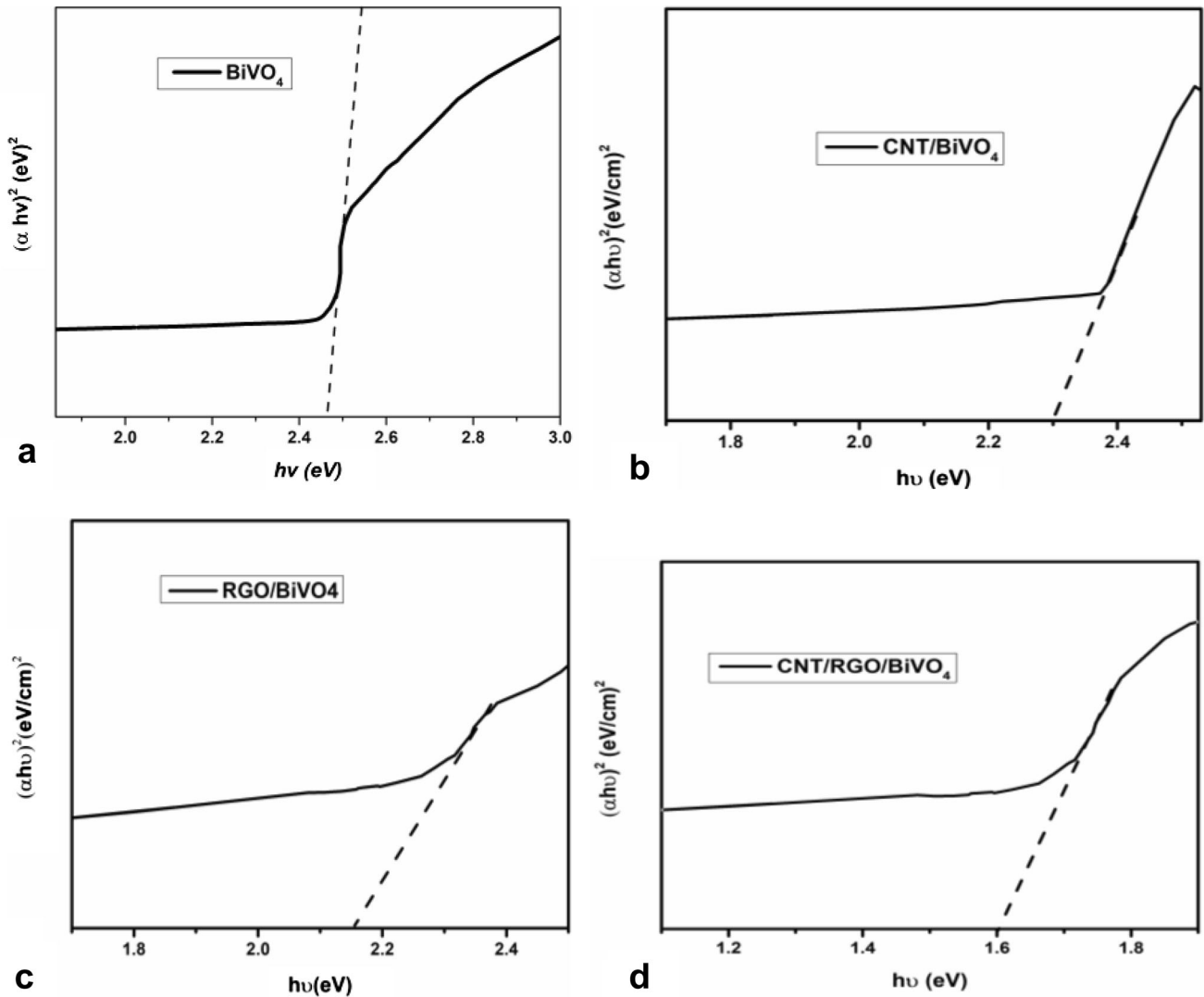


**Fig. 2** a–d Tauc plots of BiVO<sub>4</sub>, CNT/BiVO<sub>4</sub>, RGO/BiVO<sub>4</sub> and CNT/RGO/BiVO<sub>4</sub>

**Table 1** Photoelectrochemical response regarding bandgap and absorption edge

Sample	Bandgap (eV)	Absorption edge (nm)
1. Pure BiVO <sub>4</sub>	2.46	520
2. CNT/BiVO <sub>4</sub>	2.32	530
3. rGO/BiVO <sub>4</sub>	2.16	560
4. CNT/rGO/BiVO <sub>4</sub>	1.62	600

In the analysis of CNT/BiVO<sub>4</sub>, an additional peak of plane (002), is observed at 26°, representing the graphitic peak due to the tubular structure of carbon atoms. For RGO/BiVO<sub>4</sub>, a shorter peak (002) is observed at 2θ ~ 26° with decreased crystallinity which shows the successful reduction of GO into

RGO [30, 31]. Lit. survey shows that graphite and RGO, both show a peak around 26°, however, the peak of graphite is sharp, whereas the peak of RGO is very small. In the CNT/RGO/BiVO<sub>4</sub> composite (002) is observed at 26° and this is not that sharp indicating the deposition of composite. Moreover, all overlapping peaks of BiVO<sub>4</sub> in RGO/CNT/BiVO<sub>4</sub> may occur because the crystalline structure of BiVO<sub>4</sub> is larger than that of CNT and RGO.

The Linear sweep voltammetry (LSV) technique was used to analyse the photoelectrochemical response for BiVO<sub>4</sub>, RGO/BiVO<sub>4</sub>, CNT/BiVO<sub>4</sub> and RGO/CNT/BiVO<sub>4</sub> nanocomposites electrodes. A solution of 0.1 M NaNO<sub>3</sub> was used to investigate the photocurrents generated with and without light

**Fig. 3** SEM images for  $\text{BiVO}_4$  (a),  $\text{CNT/BiVO}_4$  (b),  $\text{RGO/BiVO}_4$  (c) and  $\text{CNT/RGO/BiVO}_4$  (d) electrodes

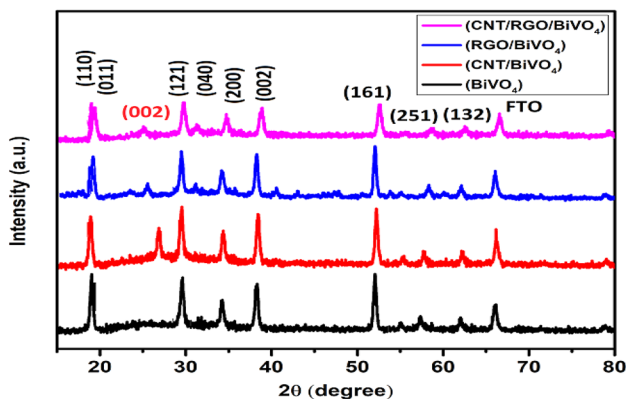
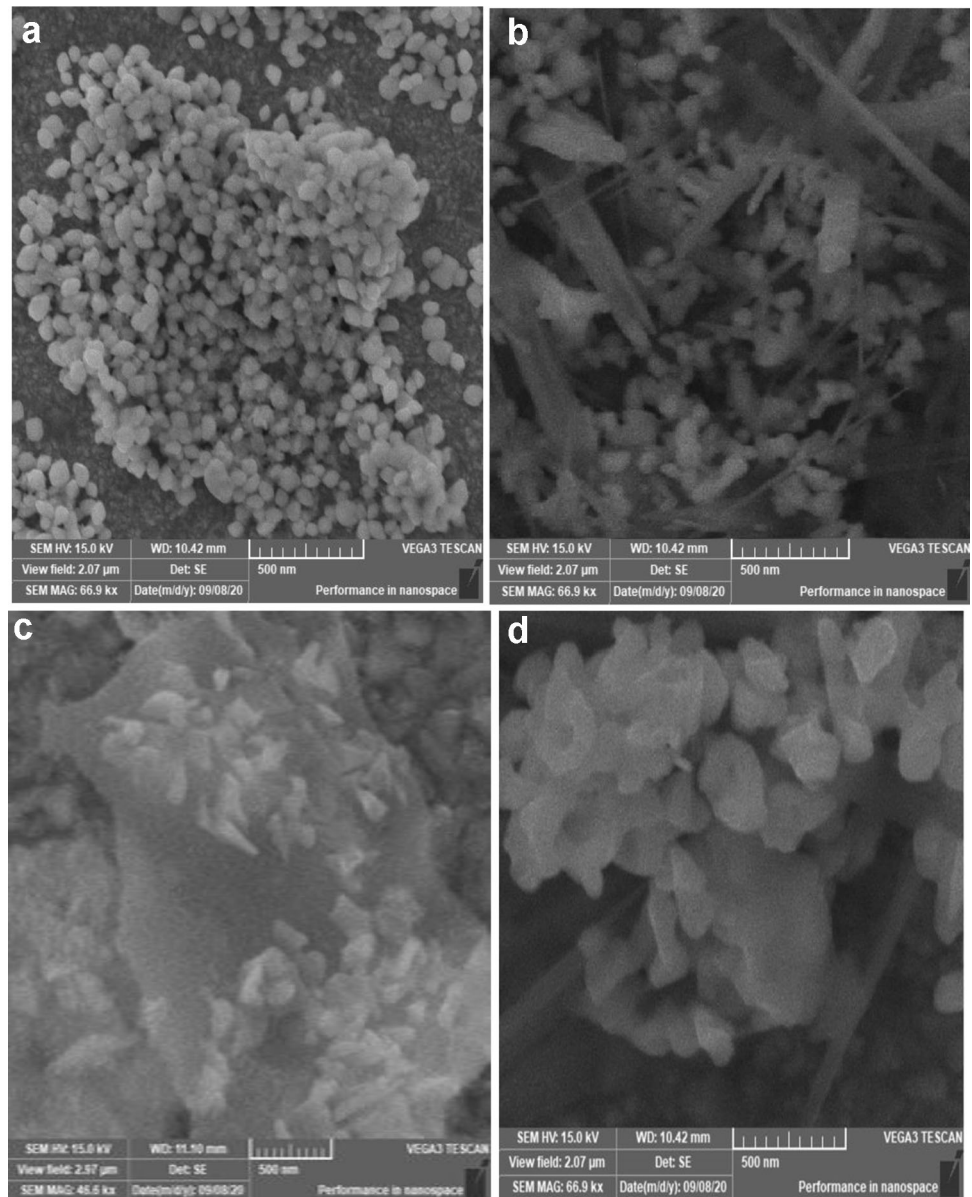


**Fig. 4** XRD patterns of  $\text{BiVO}_4$ ,  $\text{CNT/BiVO}_4$ ,  $\text{RGO/BiVO}_4$  and  $\text{CNT/RGO/BiVO}_4$  composite

irradiation. The resulting current densities plot of the above samples are shown in Fig. 5a–e, respectively.

Figure 5a shows the current density in the absence of light for  $\text{BiVO}_4$  electrode. The current is approximately  $0.25 \text{ mA cm}^{-2}$  at all increasing applied potential values showing insignificant photocurrent response.  $\text{BiVO}_4$  is a photoactive material so this graph is having no response in the absence of light. In the presence of visible light for  $\text{BiVO}_4$ , the photocurrent increases as the applied potential increases as shown in Fig. 5b [22, 31]. The maximum current density extends at  $1.35038 \text{ mA cm}^{-2}$  at  $0.6 \text{ V}$  versus SCE. In  $\text{CNT/BiVO}_4$ , upon light illumination, the current density attains the maximum value of

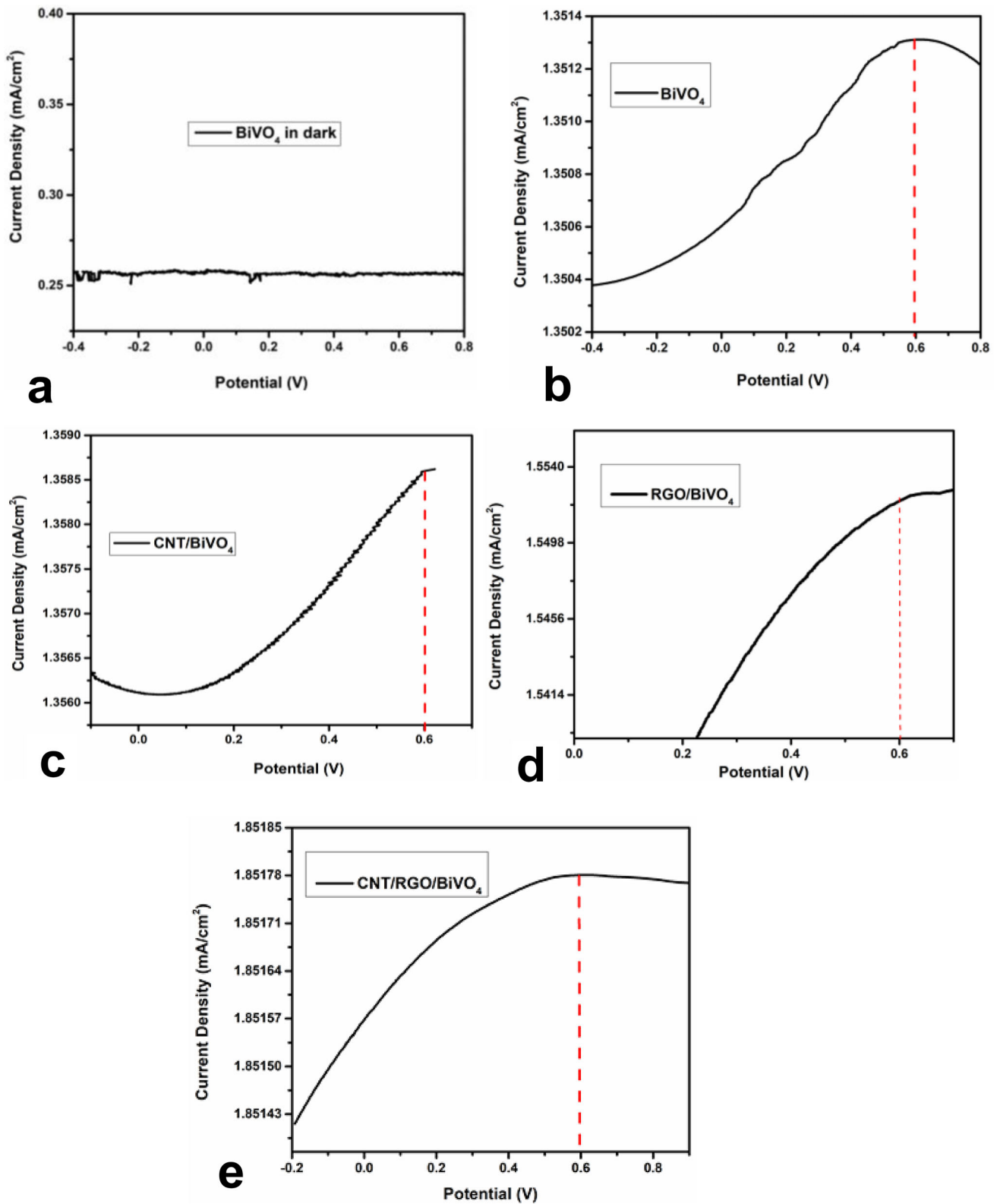


**Fig. 5** LSV analysis for BiVO<sub>4</sub> in dark (a) in light for BiVO<sub>4</sub> (b), CNT/BiVO<sub>4</sub> (c), RGO/BiVO<sub>4</sub> (d) and CNT/RGO/BiVO<sub>4</sub> (e), respectively

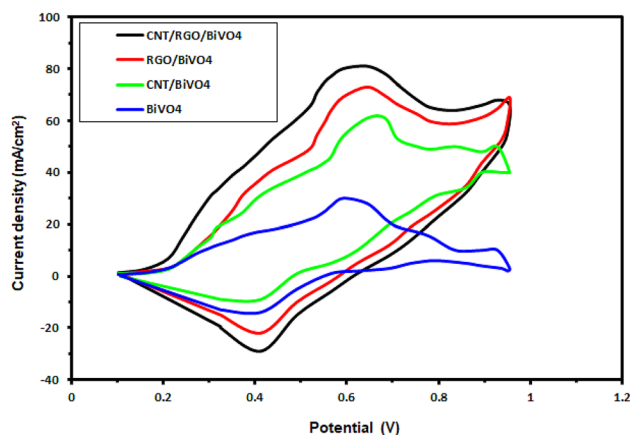


**Fig. 6** Cyclic voltammetric curves of BiVO<sub>4</sub>, CNT/BiVO<sub>4</sub>, RGO/BiVO<sub>4</sub> and CNT/RGO/BiVO<sub>4</sub> composite

1.35823 mA cm<sup>-2</sup> at 0.6 V as shown in Fig. 5c. For RGO/BiVO<sub>4</sub>, the photocurrent reaches to the maximum value of 1.53261 mA cm<sup>-2</sup> at 0.6 V as shown in Fig. 5d. For CNT/RGO/BiVO<sub>4</sub>, the maximum value of the current density is 1.85178 mA cm<sup>-2</sup> at 0.6 V as shown in Fig. 5e upon light illumination. This analysis shows the increasing trend of current density in BiVO<sub>4</sub>, CNT/BiVO<sub>4</sub>, RGO/BiVO<sub>4</sub>, and CNT/RGO/BiVO<sub>4</sub>, respectively. Upon illumination of light, the photogenerated holes in the valence band of BiVO<sub>4</sub>, with strong oxidizing ability, directly oxidizes the glucose adsorbed on the electrode surface. These electrons move through external circuit from anode to cathode and a current response is detected. When carbon nanotubes (CNT) were utilised as conducting support for BiVO<sub>4</sub> nanoparticles, it increased the photoconversion efficiency because upon light irradiation of BiVO<sub>4</sub>, when electron hole pairs are generated, then there will be more charge transfer from BiVO<sub>4</sub> to the CNTs. The interaction between BiVO<sub>4</sub> and CNT played an important role for improving photoelectrochemical response as these one dimensional materials provide faster electron transport with increased electronic conductivity. In RGO/BiVO<sub>4</sub>, graphene sheets has provided large interfaces for collection and continuous pathways for photogenerated electron transfer to the electrode surface. It is difficult to have good distribution of BiVO<sub>4</sub> nanoparticles on CNT in comparison to graphene sheet, because CNT agglomerate in bundle form. Therefore current density response of RGO/BiVO<sub>4</sub> is higher than CNT/BiVO<sub>4</sub>. In RGO/CNT/BiVO<sub>4</sub>, the composite of graphene and CNTs exhibits several benefits like the extremely conductive CNTs

specifies several routes for the transportation of electrons, which decreases the internal resistance. CNTs of 30 nm long intertwist with each other, and act as an impressive conductive binders which will hold the graphene nanosheets and the twisted CNTs on graphene nanosheets can behave such as to restrict the agglomeration of graphene nanosheets, thus enhancing the rate of electrons exchange. The increased value of the photocurrent for the composite of CNT/RGO/BiVO<sub>4</sub> confirms that this composite exhibits the tremendous photoelectrochemical response (Table 2).

### 3.1 Cyclic voltammetry

Cyclic voltammetry curves of all electrodes for the photoelectrochemical glucose oxidation were computed in 0.1 M solution of NaNO<sub>3</sub> under light irradiation and shown in Fig. 6. When glucose was added to the solution of NaNO<sub>3</sub>, oxidation peaks at about + 0.6 V, are observed as shown in Fig. 6.

The range of the potential was set from 1.0 to - 0.9 V at the scan rate of 0.1 V s<sup>-1</sup>. It is observed that anodic current peaks increases from BiVO<sub>4</sub>, to CNT/BiVO<sub>4</sub>, then to RGO/BiVO<sub>4</sub>, and finally to CNT/RGO/BiVO<sub>4</sub>. The photoelectrochemical response, observed in LSV, is also helping in the oxidation of glucose through cyclic voltammetry. Glucose is more efficiently oxidizing due to these parameters discussed in LSV analysis. Upon light irradiation electron hole pairs are generated in BiVO<sub>4</sub> and holes in the valence band helps for strong glucose oxidation at the electrodes. Electrons are transferred to electrode at a faster rate when CNT and RGO are employed in BiVO<sub>4</sub> electrode. As CNT and Graphene, both are conductive, CNTs are 1D and have faster electron transfer rate therefore significant increase in the anodic peak of CNT/RGO/BiVO<sub>4</sub> was observed. It shows that when CNT entangled on graphene sheets with BiVO<sub>4</sub> nanoparticles, it

**Table 2** Photoelectrochemical response using LSV at 0.6 V potential

	Sample	Current density (mA cm <sup>-2</sup> )
1.	BiVO <sub>4</sub>	1.35038
2.	CNT/BiVO <sub>4</sub>	1.35823
3.	RGO/BiVO <sub>4</sub>	1.53261
4.	CNT/RGO/BiVO <sub>4</sub>	1.85178



restrains the agglomeration of graphene nanosheets, and as a result rate of electron exchange increases. Glucose oxidation peak was observed at 0.6 V and the corresponding current values are increasing from sample  $\text{BiVO}_4$ ,  $\text{CNT}/\text{BiVO}_4$ ,  $\text{RGO}/\text{BiVO}_4$ ,  $\text{CNT}/\text{RGO}/\text{BiVO}_4$ , respectively, shown in Table 3.

As shown in Fig. 7a, the amperometric photocurrent of the,  $\text{BiVO}_4$ ,  $\text{CNT}/\text{BiVO}_4$ ,  $\text{RGO}/\text{BiVO}_4$  and  $\text{CNT}/\text{RGO}/\text{BiVO}_4$  electrodes have increased upon addition of glucose, and then rapidly reached a steady-state. The maximum photocurrent response during oxidation process of glucose has been detected for the  $\text{CNT}/\text{RGO}/\text{BiVO}_4$  electrode. These current responses suggest that the fabricated electrodes exhibit highly sensitive response towards the variable glucose concentration. Figure 7b shows the linear variation of glucose concentration with the current density. The glucose sensors have an excellent linear range. The correlation coefficient and sensitivity values were calculated from the graph. The slope equation for the linear curves evaluated the sensitivity values to be  $501.5 \text{ mA cm}^{-2} \text{ mM}^{-1}$ ,  $431.5 \text{ mA cm}^{-2} \text{ mM}^{-1}$ ,  $309.4 \text{ mA cm}^{-2} \text{ mM}^{-1}$ ,  $121.3 \text{ mA cm}^{-2} \text{ mM}^{-1}$  for  $\text{BiVO}_4$ ,  $\text{CNT}/\text{BiVO}_4$ ,  $\text{RGO}/\text{BiVO}_4$  and  $\text{CNT}/\text{RGO}/\text{BiVO}_4$  electrodes, respectively. Thus  $\text{CNT}/\text{RGO}/\text{BiVO}_4$  offered a visible light photoelectrochemical material with high sensitivity for non-enzymatic glucose sensing. This can be attributed to the high conductivity of graphene that successfully trapped the carbon nanotubes and nanoparticles in nanocomposite.

The high sensitivity of  $\text{CNT}/\text{RGO}/\text{BiVO}_4$  nanocomposite electrode reveals that it is highly efficient electrode for non-enzymatic glucose detection, therefore reproducibility, stability and interference test for this electrode was examined. Reproducibility of the electrode  $\text{CNT}/\text{RGO}/\text{BiVO}_4$  has been evaluated by measuring the amperometric generated current for five such similar electrodes. The relative standard deviation (RSD) of these five

**Table 3** Current density for glucose detection response using cyclic voltammetry

Sample	Current density ( $\text{mA cm}^{-2}$ )
1. $\text{BiVO}_4$	30.12321
2. $\text{CNT}/\text{BiVO}_4$	61.23124
3. $\text{RGO}/\text{BiVO}_4$	73.05235
4. $\text{CNT}/\text{RGO}/\text{BiVO}_4$	81.29234

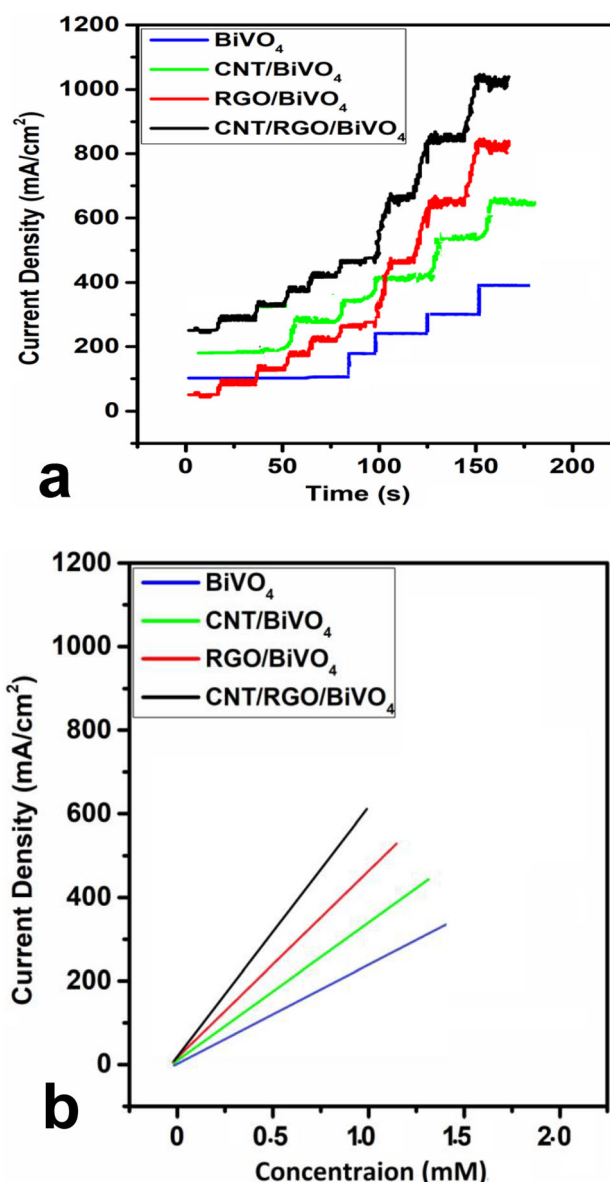


**Fig. 7** a Photocurrent responses of the  $\text{BiVO}_4$ ,  $\text{CNT}/\text{BiVO}_4$ ,  $\text{RGO}/\text{BiVO}_4$  and  $\text{CNT}/\text{RGO}/\text{BiVO}_4$  nanocomposite electrodes with the successive addition of  $10 \mu\text{M}$  glucose. b The amperometric current signal versus glucose concentration

electrodes was evaluated to be 4.1%. Thus  $\text{CNT}/\text{RGO}/\text{BiVO}_4$  electrode offers highly reproducible current for glucose detection. Inset of Fig. 8 shows the stability analysis of  $\text{CNT}/\text{RGO}/\text{BiVO}_4$  electrodes. This analysis was performed by measuring glucose detection response with 2 days interval. The magnitude of the current maintained about 90% after 23 days. This analysis examines the good stability of  $\text{CNT}/\text{RGO}/\text{BiVO}_4$  nanocomposite electrode.

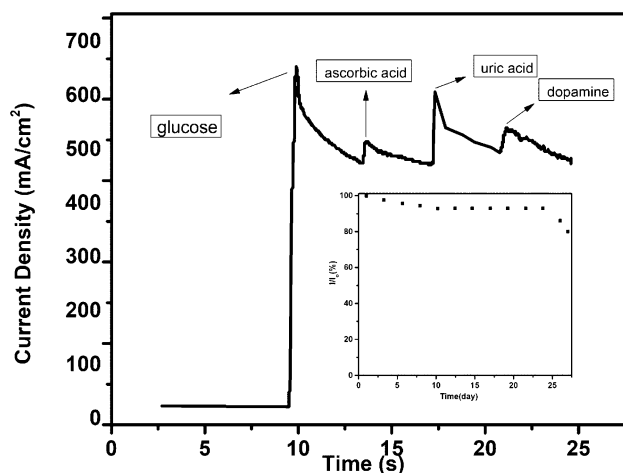


**Fig. 8** Interference response of CNT/RGO/BiVO<sub>4</sub> electrode. Inset: Stability evaluation of CNT/RGO/BiVO<sub>4</sub> electrode

In the interference analysis as shown in Fig. 8, current response was measured using intrusive species of uric acid, ascorbic acid and dopamine along with glucose. The comparison shows the major response of current signal due to glucose and negligible responses from the uric acid, ascorbic acid and dopamine. This analysis reveals that the CNT/RGO/BiVO<sub>4</sub> electrode is more sensitive for glucose in comparison to other species.

Thus CNT/RGO/BiVO<sub>4</sub> electrode is an attractive material for non-enzymatic glucose detection with high sensitivity, reproducibility and stability.

## 4 Conclusion

A successful fabrication of nanocomposites-based electrodes of BiVO<sub>4</sub>, CNT/BiVO<sub>4</sub>, RGO/BiVO<sub>4</sub>, CNT/RGO/BiVO<sub>4</sub>, was accomplished as photoelectrochemical non-enzymatic biosensor, for the recognition of glucose, by the process of electrochemical deposition. The SEM and XRD analysis revealed the surface morphology and structural analysis of nanoparticles, nanotubes, and graphene sheets. The UV visible spectroscopic results showed increasing trend in light absorption with maximum absorption for CNT/RGO/BiVO<sub>4</sub> with a bandgap of 1.6 eV. This revealed the excellent photo absorption response of CNT/RGO/BiVO<sub>4</sub> electrode due to decreased value of bandgap. This nanocomposite electrode with increased absorption spectrum excited greater number of electron hole pairs and encourages the effective charge carrier separation which decreases the rate of

recombination of electron hole pair, effectively. Under visible light irradiation, the photoelectrochemical behaviour was evaluated for all samples using Linear sweep voltammetry (LSV). The CNT/RGO/BiVO<sub>4</sub> electrode exhibited a greater photocurrent density of 1.85178 mA cm<sup>-2</sup> (v/s SCE) in comparison to other fabricated electrodes, which is credited to highly conductive property of CNTs and RGO for providing several electron transfer pathways. Glucose detection response was measured through cyclic voltammetry. An increase in anodic peak current was observed with incorporation of CNT and RGO in BiVO<sub>4</sub> nanoparticles. The maximum anodic peak current and highest sensitivity value of 501.5 mA cm<sup>-2</sup> mM<sup>-1</sup> for glucose oxidation was observed for CNT/RGO/BiVO<sub>4</sub>. The fabricated CNT/RGO/BiVO<sub>4</sub> electrode, exhibited high stability and negligible current response from the interfering species.

## Data availability

The datasets generated during and/or analysed during the current study are available from the corresponding author on reasonable request.

## Declarations

**Conflict of interest** On behalf of all authors, the corresponding author states that there is no conflict of interest.

## References

1. K.E. Toghiani, R.G. Compton, Electrochemical non-enzymatic glucose sensors: a perspective and an evaluation. *Int. J. Electrochem. Sci* **5**(9), 1246–1301 (2010)
2. S. Riaz, Obesity as a risk factor for diabetes mellitus in the local population of Pakistan. *Univ. J. Clin. Med.* **2**, 58–64 (2014)
3. S.A. Shabbir, S. Tariq, M.G.B. Ashiq, W.A. Khan, Non-enzymatic glucose sensor with electrodeposited silver/carbon nanotubes composite electrode. *Biosci. Rep.* **39**(6), BSR20181983 (2019)
4. N. Arora, Recent advances in biosensors technology: a review. *Octa J. Biosci.* **1**(2), 147–150 (2013)
5. W.W. Zhao, J.J. Xu, H.Y. Chen, Photoelectrochemical DNA biosensors. *Chem. Rev.* **114**(15), 7421–7441 (2014)

6. W.W. Zhao, J.J. Xu, H.Y. Chen, Photoelectrochemical bioanalysis: the state of the art. *Chem. Soc. Rev.* **44**(3), 729–741 (2015)
7. W.W. Zhao, J.J. Xu, H.Y. Chen, Photoelectrochemical aptasensing. *TrAC Trends Anal. Chem.* **82**, 307–315 (2016)
8. X. Zhang, Y. Guo, M. Liu, S. Zhang, Photoelectrochemically active species and photoelectrochemical biosensors. *RSC Adv.* **3**(9), 2846–2857 (2013)
9. G. Rocchitta, A. Spanu, S. Babudieri, G. Latte, G. Madeddu, G. Galleri et al., Enzyme biosensors for biomedical applications: strategies for safeguarding analytical performances in biological fluids. *Sensors* **16**(6), 780 (2016)
10. A. Devadoss, P. Sudhagar, C. Terashima, K. Nakata, A. Fujishima, Photoelectrochemical biosensors: new insights into promising photoelectrodes and signal amplification strategies. *J. Photochem. Photobiol. C* **24**, 43–63 (2015)
11. P. Guan, Y. Li, J. Zhang, W. Li, Non-enzymatic glucose biosensor based on CuO-decorated CeO<sub>2</sub> nanoparticles. *Nanomaterials* **6**(9), 159 (2016)
12. X. Zhang, F. Xu, B. Zhao, X. Ji, Y. Yao, D. Wu et al., Synthesis of CdS quantum dots decorated graphene nanosheets and non-enzymatic photoelectrochemical detection of glucose. *Electrochim. Acta* **133**, 615–622 (2014)
13. S. Komathi, N. Muthuchamy, K.P. Lee, A.I. Gopalan, Fabrication of a novel dual mode cholesterol biosensor using titanium dioxide nanowire bridged 3D graphene nanostacks. *Biosens. Bioelectron.* **84**, 64–71 (2016)
14. X. Wang, D. Liao, H. Yu, J. Yu, Highly efficient BiVO<sub>4</sub> single-crystal photocatalyst with selective Ag<sub>2</sub>O-Ag modification: orientation transport, rapid interfacial transfer and catalytic reaction. *Dalton Trans.* **47**(18), 6370–6377 (2018)
15. J. Fang, L. Xu, Z. Zhang, Y. Yuan, S. Cao, Z. Wang et al., Au@TiO<sub>2</sub>-CdS ternary nanostructures for efficient visible-light-driven hydrogen generation. *ACS Appl. Mater. Interfaces* **5**(16), 8088–8092 (2013)
16. M. Ge, Y. Li, L. Liu, Z. Zhou, W. Chen, Bi<sub>2</sub>O<sub>3</sub>-Bi<sub>2</sub>WO<sub>6</sub> composite microspheres: hydrothermal synthesis and photocatalytic performances. *J. Phys. Chem. C* **115**(13), 5220–5225 (2011)
17. T.W. Kim, K.S. Choi, Nanoporous BiVO<sub>4</sub> photoanodes with dual-layer oxygen evolution catalysts for solar water splitting. *Science* **343**(6174), 990–994 (2014)
18. Y. Chen, G. Tian, Y. Shi, Y. Xiao, H. Fu, Hierarchical MoS<sub>2</sub>/Bi<sub>2</sub>MoO<sub>6</sub> composites with synergistic effect for enhanced visible photocatalytic activity. *Appl. Catal. B* **164**, 40–47 (2015)
19. L. Zhou, W. Wang, H. Xu, S. Sun, M. Shang, Bi<sub>2</sub>O<sub>3</sub> hierarchical nanostructures: controllable synthesis, growth mechanism, and their application in photocatalysis. *Chem. A Eur. J.* **15**(7), 1776–1782 (2009)
20. A.I. Gopalan, N. Muthuchamy, K.P. Lee, A novel bismuth oxychloride-graphene hybrid nanosheets based non-enzymatic photoelectrochemical glucose sensing platform for high performances. *Biosens. Bioelectron.* **89**, 352–360 (2017)
21. V.H. Nguyen, Q.T.P. Bui, D.V.N. Vo, K.T. Lim, L.G. Bach, S.T. Do et al., Effective photocatalytic activity of sulfate-modified BiVO<sub>4</sub> for the decomposition of methylene blue under LED visible light. *Materials* **12**(17), 2681 (2019)
22. J. Sun, C. Wang, T. Shen, H. Song, D. Li, R. Zhao, X. Wang, Engineering the dimensional interface of BiVO<sub>4</sub>-2D reduced graphene oxide (RGO) nanocomposite for enhanced visible light photocatalytic performance. *Nanomaterials* **9**(6), 907 (2019)
23. D.K. Lee, I.S. Cho, S. Lee, S.T. Bae, J.H. Noh, D.W. Kim, K.S. Hong, Effects of carbon content on the photocatalytic activity of C/BiVO<sub>4</sub> composites under visible light irradiation. *Mater. Chem. Phys.* **119**(1–2), 106–111 (2010)
24. A. Zhang, J. Zhang, Characterization and photocatalytic properties of Au/BiVO<sub>4</sub> composites. *J. Alloys Compd.* **491**(1–2), 631–635 (2010)
25. S. Xiong, T. Wu, Z. Fan, D. Zhao, M. Du, X. Xu, Preparation of a leaf-like BiVO<sub>4</sub>-reduced graphene oxide composite and its photocatalytic activity. *J. Nanomater.* **2017**, 1–2 (2017)
26. Y.H. Ng, A. Iwase, A. Kudo, R. Amal, Reducing graphene oxide on a visible-light BiVO<sub>4</sub> photocatalyst for an enhanced photoelectrochemical water splitting. *J. Phys. Chem. Lett.* **1**(17), 2607–2612 (2010)
27. S. Woo, Y.R. Kim, T.D. Chung, Y. Piao, H. Kim, Synthesis of a graphene-carbon nanotube composite and its electrochemical sensing of hydrogen peroxide. *Electrochim. Acta* **59**, 509–514 (2012)
28. J. Su, X.X. Zou, G.D. Li, X. Wei, C. Yan, Y.N. Wang et al., Macroporous V<sub>2</sub>O<sub>5</sub>-BiVO<sub>4</sub> composites: effect of heterojunction on the behavior of photogenerated charges. *J. Phys. Chem. C* **115**(16), 8064–8071 (2011)
29. X. Gao, H.B. Wu, L. Zheng, Y. Zhong, Y. Hu, X.W. Lou, Formation of mesoporous heterostructured BiVO<sub>4</sub>/Bi<sub>2</sub>S<sub>3</sub> hollow discoids with enhanced photoactivity. *Angew. Chem. Int. Ed.* **53**(23), 5917–5921 (2014)
30. S. Li, J.X. Xiong, C.X. Chen, F.Q. Chu, Y. Kong, L.H. Deng, Amperometric biosensor based on electrochemically reduced graphene oxide/poly(m-dihydroxybenzene) composites for glucose determination. *Mater. Technol.* **32**(1), 1–6 (2017)
31. S. Wang, S. Li, W. Wang, M. Zhao, J. Liu, H. Feng et al., A non-enzymatic photoelectrochemical glucose sensor based on BiVO<sub>4</sub> electrode under visible light. *Sens. Actuators B Chem.* **291**, 34–41 (2019)

**Publisher's Note** Springer Nature remains neutral with regard to jurisdictional claims in published maps and institutional affiliations.